Songklanakarin J. Sci. Technol.
41 (1), 109-116, Jan. – Feb. 2019

http://www.sjst.psu.ac.th

Original Article

CFD analysis of thermal performance of microchannel nanofluid flow at different Reynolds numbers

Arjun Kozhikkatil Sunil* and Rakesh Kumar

Department of Mechanical Engineering, Indian Institute of Technology (ISM), Dhanbad, 826004 India

Received: 28 March 2017; Revised: 4 September 2017; Accepted: 4 October 2017

Abstract

Convective heat transfer and pressure drop using alumina-water nanofluid under laminar and turbulent flow regimes using the viscous laminar model and standard k-ε model have been studied. A circular microchannel heat exchanger (0.1 m long and 0.5 mm inner diameter) with constant wall temperatures, and 0 to 5% Al_2O_3-water nanofluid flowing inside and cold water flowing outside was used. This experiment showed that convection heat transfer increased remarkably with the increase of nanoparticle concentration under various values of Reynolds numbers. The heat transfer coefficient increased 15% compared to pure water under 5% volume concentration for the laminar regime and 12% for the turbulent zone (Nusselt number decreased about 2.5%). The pressure drop of the nanofluid increased as the volume concentration increased. However, compared with pure water, the change in pressure drop was significant. Therefore, the use of a nanofluid has a great penalty on pressure drop.

Keywords: circular microchannels, alumina-water nanofluids, computational fluid dynamics, heat transfer coefficient, pressure drop.

1. Introduction

In recent years, research in the field of single-phase and two-phase flow heat transfer at a micro-scale level has been constantly increasing due to the rapid growth of technology applications that need the transfer of heat at high rates in a relatively small space and volume. Such applications span from compact heat exchangers to cooling systems for computer CPUs to microfluidic devices. Conductivity of suspended nano-particles in conventional fluids is found to be greater than the conventional fluids and this motivated many to research its application in heat exchangers. The large surface area of nanoparticles allows for more heat transfer. Another advantage is the mobility of the particles that is attributed to the tiny size, which may bring about micro-convection of fluid and increased heat transfer. Because of the small particles, they weigh less and the chances of sedimentation are less. This will make the mentation are less. This will make the nanofluids more stable. Large enhancement of conductivity was achieved with a very small concentration of particles that completely maintained the Newtonian behaviour of the fluid. The rise in viscosity was nominal; hence, pressure drop increased only marginally. Unlike the situation with micro-slurries, the enhancement of conductivity was found to depend not only on particle concentration but also on particle size. In general, with decreasing particle size, an increase in enhancement was observed (Das, Choi, & Patel, 2006; Hasan, 2011; Peygham barzadeh & Hashemabadi, 2011; Hung, Yan, Wang, & Chang, 2012a, 2012b).

Very good and updated reviews of these aspects were already reported (Morini, 2004, 2006). Scaling effects, which play a relevant role in micro-scale single-phase flow heat transfer, are viscous heating, thermal entrance length, and axial conduction (conjugate heat transfer). Micro-scale heat transfer in liquid single-phase flow, both for laminar and turbulent flow, can be well predicted using what is known from the knowledge of heat transfer in macro-scale, i.e. Nusselt number (Nu) = 4.36 for laminar flow and the Gnielinski (1976) correlation for turbulent flow. With 1-5 volume percent nanoparticle

*Corresponding author
Email address: arjun@mece.ism.ac.in

concentrations, the thermal conductivity of the suspensions can increase more than 20% (Lee, Choi, Li, & Eastman, 1999). Forty percent heat transfer enhancement was found with Al_2O_3 particles (Heris, Etemadand, & Esfahany, 2006). Heat transfer enhancement increases with particle volume concentration (Bianco, Chiacchio, Manca, & Nardini, 2009). Nanofluids increase the heat transfer coefficient by 15% and 12% in comparison to its base fluids in laminar and turbulent zones, respectively (Arjun & Rakesh, 2016). Convective heat transfer coefficient for nanofluids with a volume fraction of 0.03 was found to be 12% lower than pure water (Pak & Cho, 1998). However, opposite conclusions were also reported (Lee, Choi, Li, & Eastman, 1999; Xuan & Li, 2003; Wen & Ding, 2005).

By increasing particle volume fraction, degree of synergy between the velocity and temperature fields of nanofluid flows can be intensified, leading to similar convection heat transfer enhancement, even if the thermal conductivities of nanoparticles are quite different (Minea & Manca, 2017). The augmented thermal conductivity of nanofluids through the synergistic effect of promising properties of all of its constituents is considered to be the driving factor for enhanced heat transfer performance (Minea, 2017a). The Nu correlation equation as a function of Reynolds number (Re), Prandtl number (Pr), and nanoparticle concentration is more reliable because discrepancies exist in viscosity mainly due to insufficient methods of estimation, and confirmation of at least a 12% increased thermal conductivity was obtained (Minea, 2017b).

The strength of numerical simulations is the possibility to investigate small details that are impossible to observe in experiments. Computational fluid dynamics (CFD) modelling and simulation of single-phase circular micro-channel flow and conjugate heat transfer, which couples fluid convection and heat conduction in solids, is validated in this study by comparing data from an experimental investigation (Lee & Mudawar, 2007) and a parameter sensitivity study of the microchannel. In this work, the heat transfer coefficient and pressure drop of water-based nanofluids of Al_2O_3 were characterised in a circular microchannel of 0.1 m length and diameter of 0.5 mm. The simulations were performed for different nanoparticle volume concentrations (0-5%) and flow rates ($0.00009<Re<11980$). The nanofluid temperatures have also been specifically analyzed and discussed.

The effects of Re and Peclet (Pe) numbers on the flow behaviour in circular microchannels were not found specifically in previous reports. In previous work, agreement of computed temperatures and heat transfer coefficients were not reported within an acceptable limit of the analytical values. The effect of change of temperature from inlet to outlet with the Re number was not found in previous literature. The effect of temperature distribution with respect to radial position of the Pe number was not reported previously. Only very few reports are available with respect to the effect of pressure drop with the Re number. The dependency of entrance length for fully developed flow on nanoparticle concentrations was not proved conclusively in the previous work. The effect of wall temperature for higher Re numbers due to greater value of a Pe number in a circular microchannel was not previously reported. The effect of Re number and Pe number on the flow behaviour in circular microchannels was found. The use of nanofluids as the heat transport medium in the channel were found useful both in laminar and in turbulent flow conditions. CFD modelling and simulation of single-phase circular micro-channel flow and conjugate heat transfer were not studied for a wide range of Re numbers.

2. Numerical Modelling and Validation

The geometry of a circular microchannel with structured mesh is shown in Figures 1 and 2 with 100×10 nodes. Based on $Re=Dv\rho/\mu$, either viscous laminar model at $Re<2000$ or standard κ-ε model at $Re>2000$ is used for single-phase laminar and turbulent flow. D is the diameter of the microchannel, ρ and μ are the density and viscosity of the fluid. The density, heat capacity, and thermal conductivity of alumina are 3600 kg/m^3, 765 J/kgK, and 36 W/mK, respectively. The properties of the nanofluids (nf) at 30 °C and 100 kPa were used.

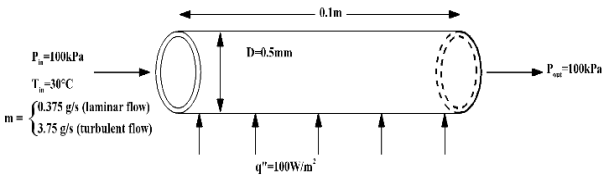

Figure 1. Fluid flow through a circular microchannel.

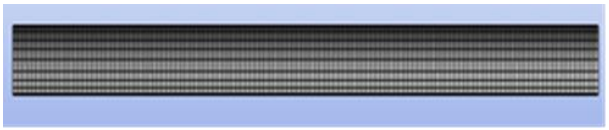

Figure 2. 2D geometry with structured mesh.

A pressure correction based iterative SIMPLE algorithm with 1st order upwind scheme for discretizing the convective transport terms and a no slip boundary condition for non-porous wall surfaces and 2D axis symmetry at centerline were assigned and hence not modeled as a volume. It is assumed that the continuum hypothesis is valid. The equation for conservation of mass, or continuity equation, can be written as follows:

$$\frac{\partial \rho}{\partial t} + \nabla \cdot (\rho \vec{v}) = S_m \quad (1)$$

where S_m is the mass added to continuous phase from dispersed second phase and any user defined sources.

Equation 1 is the general form of the mass conservation equation and is valid for both incompressible compressible flows.

Conservation of momentum in an inertial (non-accelerating) reference frame is described by:

$$\frac{\partial}{\partial t}(\rho \vec{v}) + \nabla \cdot (\rho \vec{v} \vec{v}) = -\nabla p + \nabla \cdot (\bar{\bar{\tau}}) + \rho \vec{g} + \vec{F} \quad (2)$$

where p is the static pressure, $\bar{\bar{\tau}}$ is stress tensor, $\rho\vec{g}$ and $\vec{F}$ are gravitational and external body forces (that arise from interaction with the dispersed phase), respectively. $\vec{F}$ also contains other model dependent source terms such as porous-media and user-defined sources.

The stress tensor $\bar{\bar{\tau}}$ is given by:

$$\bar{\bar{\tau}} = \mu\left((\nabla\vec{v} + \nabla\vec{v}^T) - 2/3 \cdot \vec{v}I\right) \tag{3}$$

where μ is the molecular viscosity, I is the unit tensor and second term on right side is effect of volume dilation.

ANSYS FLUENT solves the energy equation in the following form:

$$\frac{\partial}{\partial t}(\rho E) + \nabla \cdot \left(\vec{v}(\rho E + p)\right) = \nabla \cdot \left(\kappa_{eff}\nabla T - \sum_j h_j\overrightarrow{J_j} + \left(\bar{\bar{\tau}}_{eff} \cdot \vec{v}\right)\right) + S_h \tag{4}$$

κ_{eff} is effective conductivity (κ+κt, where κt is turbulent thermal conductivity), $\overrightarrow{J_I}$ is diffusion flux, S_h is heat of chemical reaction. The first three terms on the right-hand side of Equation represent energy transfer due to conduction, species diffusion, and viscous dissipation, respectively. Viscous laminar and standard k-ε models are used to predict the steady temperature in laminar and turbulent zone (Arjun & Rakesh, 2017).

$$E = h - \frac{p}{\rho} + \frac{v^2}{2} \tag{5}$$

where sensible enthalpy h is defined as

$$h = \sum_j Y_j h_j \tag{6}$$

where Y_j is the mass fraction of species j.

$$h_j = \int_{T_{ref}}^{T} c_{p,j}dT \tag{7}$$

T_{ref} used is 298.15 K.

At both hydraulic and thermally fully developed condition, Nu is constant for laminar flow.

$$\frac{hD}{\kappa} = 4.36 \Rightarrow h \approx \kappa\kappa \tag{8}$$

and follows Dittius-Boelter equation for turbulent flow (Lee, Choi, Li, & Eastman, 1999).

$$\frac{hD}{\kappa} = 0.023\left(\frac{Dv\rho}{\mu}\right)^{0.8}\left(\frac{C_p\mu}{\kappa}\right)^{0.4} \Rightarrow h \approx \kappa^{0.6}\upsilon^{0.8}\mu^{-0.4} \tag{9}$$

From Equations 8 and 9, it is clear that thermal conductivity has a greater effect on heat transfer coefficient for laminar flow compared to turbulent flow. This implied that the enhancement effect, due to the increased thermal conductivity of the nanofluids, is significantly weaker for turbulent flow than for laminar flow. The enhancement in turbulent flow is also dependent on the flow rate in addition to viscosity and specific heat. Since $h \approx \kappa^{0.6}\mu^{-0.4}Cp^{0.4}$ and because increased nanoparticle concentration enhances viscosity and degrades specific heat, the enhancement effect of nanoparticles in turbulent flow is further reduced compared to thermal conductivity alone.

For 2D axis symmetric geometries, the continuity equation (Pak & Cho, 1998) is:

$$\frac{\partial\rho}{\partial t} + \frac{\partial}{\partial x}(\rho v_x) + \frac{\partial}{\partial r}(\rho v_r) + \frac{\rho v_r}{r} = 0 \tag{10}$$

where x is the axial coordinate in the flow direction, r is the radial coordinate, and υ_x and υ_ρ are the axial and radial velocities. For 2D axis symmetric geometries, the axial and radial momentum conservation equations are given by:

$$\frac{\partial}{\partial t}(\rho v_x) + \frac{1}{r}\frac{\partial}{\partial x}(r\rho v_x v_x) + \frac{1}{r}\frac{\partial}{\partial r}(r\rho v_r v_x) = \frac{-\partial p}{\partial x} + \frac{1}{r}\frac{\partial}{\partial x}\left[r\mu\left(2\frac{\partial v_x}{\partial x} - \frac{2}{3}(\nabla\cdot\vec{v})\right)\right] + \frac{1}{r}\frac{\partial}{\partial r}\left[r\mu\left(\frac{\partial v_x}{\partial r} + \frac{\partial v_r}{\partial v_x}\right)\right] + F_x \tag{11}$$

$$\frac{\partial}{\partial t}(\rho v_r) + \frac{1}{r}\frac{\partial}{\partial x}(r v_x v_r) + \frac{1}{r}\frac{\partial}{\partial r}(r v_r v_r) = \frac{-\partial\rho}{\partial r} + \frac{1}{r}\frac{\partial}{\partial x}\left[r\mu\left(\frac{\partial v_r}{\partial x} + \frac{\partial v_x}{\partial r}\right)\right]$$

$$+\frac{1}{r}\frac{\partial}{\partial r}\left[r\mu\left(2\frac{\partial v_r}{\partial r} - \frac{2}{3}(\nabla\cdot\vec{v})\right)\right] - 2\mu\frac{v_r}{r^2} + \frac{2}{3}\frac{\mu}{r}(\nabla\cdot\vec{v}) + \rho\frac{v_z^2}{r} + F_r \tag{12}$$

$$\nabla\cdot\vec{v} = \frac{\partial v_x}{\partial x} + \frac{\partial v_r}{\partial r} + \frac{v_r}{r} \tag{13}$$

Since the microchannel with small radial thickness is horizontally placed, F is taken as zero. The standard k-ε model is used to model single-phase turbulent flow. The turbulence kinetic energy, k, and its rate of dissipation, ε, are obtained solving the following transport equations:

$$\frac{\partial}{\partial t}(\rho k) + \frac{\partial}{\partial x_i}(\rho k v_i) = \frac{\partial}{\partial x_j}\left[\left(\mu + \frac{\mu_t}{\sigma_k}\right)\frac{\partial k}{\partial x_j}\right] + G_k + G_b - \rho\varepsilon - Y_M + S_k \quad (14)$$

$$\frac{\partial}{\partial t}(\rho \varepsilon) + \frac{\partial}{\partial x_i}(\rho \varepsilon v_i) = \frac{\partial}{\partial x_j}\left[\left(\mu + \frac{\mu_t}{\sigma_\varepsilon}\right)\frac{\partial \varepsilon}{\partial x_j}\right] + C_{1\varepsilon}\frac{\varepsilon}{k}(G_k + C_{3\varepsilon}G_b) - C_{2\varepsilon}\rho\frac{\varepsilon^2}{k} + S_\varepsilon \quad (15)$$

G_k and G_b are turbulence kinetic energy due to mean velocity gradients and buoyancy, Y_M is fluctuating dilatation, $C_{1\varepsilon}$, $C_{2\varepsilon}$, and $C_{3\varepsilon}$ are constants, σ_k and σ_ε are turbulent Pr, S_k and S_ε are user-defined source terms.

Turbulent viscosity is computed by combining k and ε as provided (Wen & Ding, 2005).

$$\mu_t = \rho C_\mu \cdot \frac{k^2}{\varepsilon} \quad (16)$$

$C_{1\varepsilon}$=1.44, $C_{2\varepsilon}$=1.92, C_μ=0.09, σ_k= 1.0, and σ_ε= 1.3. $C_{3\varepsilon}$ has values 1 (along) or 0 (perpendicular) for flow direction with gravity. The governing equation for energy is the same as represented in Equation 4. The bulk mean temperature, $T_{m,x}$ and wall temperature, $T_{w,x}$ with distance x from the microchannel entrance can be obtained by doing the thermal energy balance around the microchannel (Lee & Mudawar, 2007) in the following equations.

$$T_{m,x} = T_{in} + \frac{q^{"}\pi D x}{m C_{p,nf}} \quad (17)$$

$$T_{w,x} = T_{m,x} + \frac{q^{"}}{h} \quad (18)$$

where $T_{m,x}$ and $T_{w,x}$ are bulk mean and wall temperature, The inlet temperature T_{in} is 303.15 K, q" is the heat flux, x is the axial distance and h is heat transfer coefficient.

To characterize the effect of fluid flow on the thermal behaviour of the microchannel heat exchanger, The Pe number is defined as:

$$Pe = \frac{\rho_f C_{p,f} u}{\frac{\kappa}{L}} \quad (19)$$

A no slip boundary condition for wall surfaces, i.e. $\upsilon_x = \upsilon_\rho = 0$, and axis symmetry at centerline was assigned and the Knudsen number was found to be 4.3×10^{-6}. Pure water as base fluid and alumina as nanoparticles of 23 nm average diameter were used, this makes the single phase flow assumption valid. The specified solver uses a pressure correction based iterative SIMPLE algorithm with 1st order upwind scheme for discretizing convective transport terms. The values obtained from current methods (Ansys, 2013) were used to compare the experimental values already reported (Lee & Mudawar, 2007).

Grid sizes tested were 100x12, 100x18, and 100x24. Mesh configurations of 100x18 have wall y+ values resolved in the region, $7 < y+ < 8$ and values close to $y+ \approx 8$ ensured most desirable grid independence. This method is highly acceptable since excellent agreement between the simulated and experimental data was obtained with a mean absolute error of 0.008% for laminar flows and 0.048% for turbulent flows. The analytical and computational Nu numbers obtained for laminar and turbulent flow of 0 to 5% nanofluids proved that the CFD results well predicted the analytical Nu numbers. The presented simulated values showed 99.73% and 100% accuracy to predict the analytical values of heat transfer coefficient in the experimental results for laminar and turbulent flows, respectively, using sum of squares error. A good regression analysis with R^2 0.9998*** and 1*** for laminar and turbulent flows between the simulated values and experimental results were also obtained (Gnielinski, 1976).

3. Results and Discussion

It was observed that as the Re number increased, the pressure drop increased. A linear variation of pressure was observed with axial distance at all Re numbers for all nanofluid volume concentrations. The pressure drops of Al_2O_3-water nanofluids were found to be approximately the same as water at Re=5 and below and implies that the nanofluid incurs no penalty of pump power and may be suitable for practical application. However, above Re=5, the pressure drop of Al_2O_3-water nanofluids were higher than water. This observation was in accordance with pumping power requirement of alumina/water nanofluid nearly equal to water for the same Pe number (Raja, Arunachalam, & Suresh, 2012) and pressure loss increased only slightly with the increase in volume concentration of nanofluids (Das, Putra, Thiesen, & Roetzel, 2003). Velocity had no variation from inlet to exit, except for the entrance length which indicated that the circular microchannel is at the fully developed flow condition.

The analytical and computational Nu numbers for turbulent flow of 0 to 5% Al_2O_3-water nanofluids at Re=11980 proved that the CFD results well predicted the analytical Nu numbers (Figure 3). Pressure drop also showed similar results using water and 2% nanofluid at Re=0.1 to 500 (Figure 4). As Re increased, the pressure drop also increased for both water and nanofluids. The pressure drop increased 281% using the 2% Al_2O_3-water nanofluid compared to the base fluid. In the case of laminar flow, the heat transfer coefficient increased by 15% from 0 to 5% alumina-water nanofluid (Figure 5), and in turbulent flow, the heat transfer coefficient increased by 12%, but the decrease of the Nu number was 2.5% (Figure 3). The enhancement of heat transfer in laminar flow is greater compared to turbulent flow but the use of nanoparticles in either laminar or turbulent conditions was found to be beneficial. A greater heat transfer coefficient is obtained at the circular microchannel entrance. The entrance length increases with increases in the Re number. These results were in agreement with the results reported by Bianco, Manca, & Nardini (2011) but contradicted the results obtained by Lee & Mudawar (2007) who opined that heat transfer enhancement was negligible in turbulent alumina-water nanofluid flow in a circular microchannel.

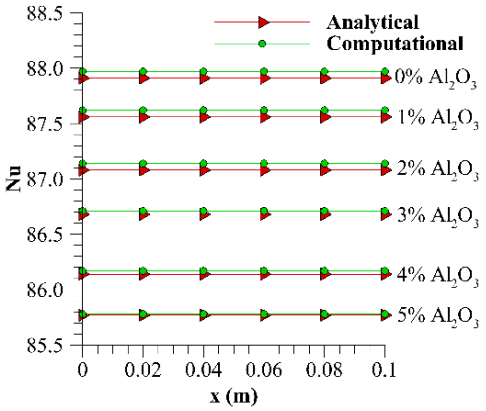

Figure 3. Comparison of analytical and computational Nu for a nanofluid at Re=11980.

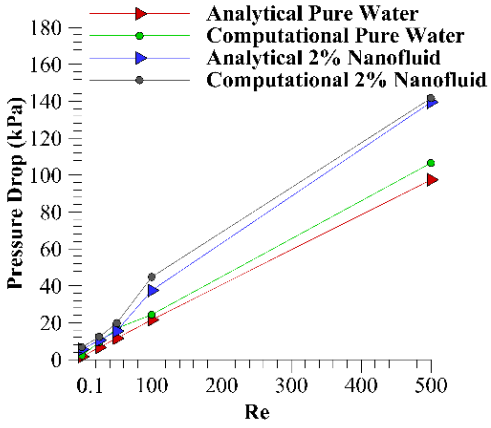

Figure 4. Comparison of analytical and computational pressure drop of water and nanofluid at Re=0.1-500.

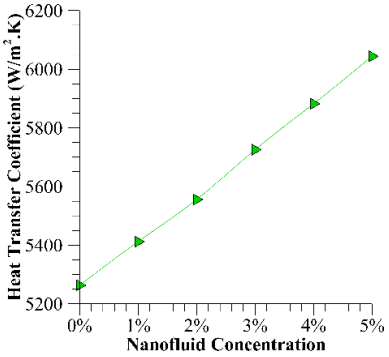

Figure 5. Heat transfer coefficients for 0-5% nanofluid at Re=1198.

Nanofluids improved the heat transfer coefficient by an increase of 12.2% even though the Nu number decreased by 2.5%. This is because the Nu number depends upon both the thermal conductivity and the heat transfer coefficient. Though the thermal conductivity and heat transfer coefficient are both higher for the nanofluid by about 14.9% and 12.2%, respectively, compared to the base fluid, the larger increase in the thermal conductivity than the increase in heat transfer coefficient led to a drop in the Nu number of about 2.5% for the nanofluid. The relationship between the thermal conductivity, heat transfer coefficient, and Nu number for the base and nanofluid cases can be illustrated by the definition of the Nu number (Equation 9). These results quantify the possible increase in both the conductive and convective heat transfer modes and hence confirm the potential of nanofluids as effective coolants.

The heat transfer coefficient values were found to be independent of axial position which meant that a circular microchannel is at the fully thermal developed condition in both laminar and turbulent types of flows. The value of Pe for both Re=1198 and Re=11980 were much greater than one, and hence temperature at all points on the x-axis were equal to inlet temperature. A substantial change in temperature from inlet to outlet was observed at Re=0.00009 with respect to axial distance from the inlet (Figure 6). The percent change in temperature starts to drop from the axial distance position of 0.07 m and tends to zero after 0.1 m. It was also noticed that the use of water results in a higher wall temperature than its nanofluids. Furthermore, the wall temperature at a particular axial position decreased as the nanoparticle concentrations increased, which might be due to the combined effects of density, viscosity, and thermal conductivity. The effect of Re number on the variation of nanofluid temperature with axial position showed less variation in nanofluid temperature with axial distance at Re greater than 1 and no change at still higher Re numbers. The Pe number increased with an increase in Re number and thus the contribution of convective heat flux dominated over conductive heat flux at higher Re numbers and inlet temperature of fluid penetrates more towards the outlet at higher Pe numbers.

There was no variation of nanofluid temperature with radial position. The nanofluid temperatures at different axial distances and Re=0.1-50 are shown in Figure 7. As Re increased, temperature decreased. The temperature increased from inlet to outlet at Re numbers below 50. Convective heat transfer rate dominates over conductive heat transfer rate even

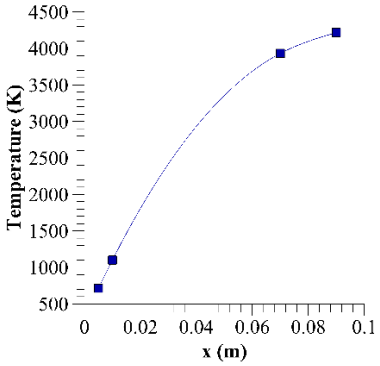

Figure 6. Temperature of 1% nanofluid at Re=0.00009.

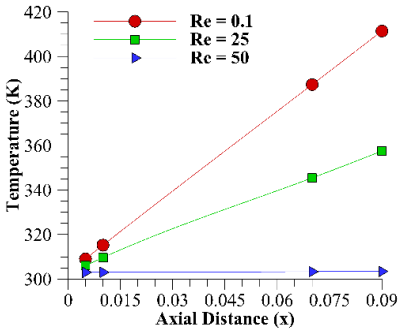

Figure 7. Temperature of 1% nanofluid at Re=0.1-50. The temperature contour plots along the

at Re=0.1 for which also Pe>>1. However, at very a low Re number, the Pe number is much less than 1 and the conductive heat transport dominates over convective heat transfer and variation of the temperature of the nanofluid is very high. However, no radial temperature distribution was observed because the diameter of the channel is very much less compared to the length. The wall temperature increased within the flow direction of the circular microchannel at very low Re numbers. Wall temperature had negligible variation for higher Re numbers due to the higher Pe number.

The temperature contour plots along the microchannel are shown Figures 8 and 9 at Re numbers of 100 and 500, which support the different temperature profiles reported by earlier studies.

The temperature profile remained parabolic in the fully developed region. The temperature contour plots showed that at lower Re numbers, there was a distribution of temperature in the transverse direction. However, at high Re numbers, because of the high Pe number, the inlet temperature almost reached the outlet temperature around the centreline and some temperature distributions are observed in the transverse direction only very near to the wall. As Re numbers increased, the temperature profile differed towards the exit.

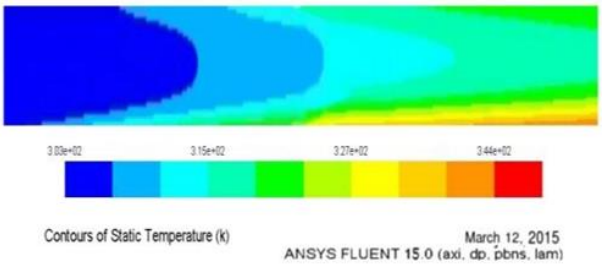

Figure 8. Temperature contour plot at Re=100.

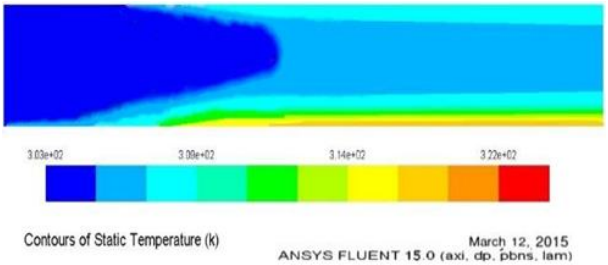

Figure 9. Temperature contour plot at Re=500.

4. Conclusions

We reported the effect of nanofluid for different volumetric concentrations of 0-5% at Re numbers of 0.00009-11980 and Pe below and above unity in heat transfer enhancement in terms of heat transfer coefficient and corresponding Nu and ΔP in a circular microchannel. The effect of change of fluid temperature from inlet to outlet using 1% nanofluid for lower Re numbers of 0.00009-50 as well as temperature contours at Re=100 and Re=500 were also reported. Convective heat transfer of the Al_2O_3-water nanofluid was significantly higher than pure water. The convective heat transfer increased as the Re number and volume concentration increased. The pressure drop of the Al_2O_3-water nanofluid was much higher than pure water in the given conditions. This implied that the nanofluid incurred great penalty in pump power and it was not suitable for practical applications. The use of nanofluids as a heat transport medium in a circular microchannel was found useful both in laminar and in turbulent flow conditions in the present investigation. The computed temperatures and heat transfer coefficients were found to be in close agreement with the analytical values. The change of temperature from inlet to outlet was found to increase with decreasing Reynolds numbers. Temperature distribution was found independent of radial position even at a very low value of Pe number. Pressure drop increased with an increase in Reynolds number. The entrance length for a fully developed flow depends on the nanoparticle concentration. Wall temperature had negligible variation for higher Reynolds numbers due to the greater value of Pe number in a circular microchannel.

References

Ansys. (2013). *ANSYS fluent 15.0 theory guide*. Canonsburg, PA: Ansys.

Arjun, K. S., & Rakesh, K. (2016). Hydrodynamics and heat transfer analysis of nanofluids flow in a circular micro channel by simulations. *Computational Thermal Sciences: An International Journal, 8*(2), 193-208. doi:10.1615/ComputThermalScien.2016013798

Arjun, K. S., & Rakesh, K. (2017). Heat transfer enhancement using alumina nanofluid in circular micro channel. *Journal of Engineering Science and Technology, 12*(1), 265-279.

Bianco, V., Chiacchio, F., Manca, O., & Nardini, S. (2009). Numerical investigation of nanofluids forced convection in circular tubes. *Applied Thermal Engineering, 29*, 3632-3642. doi:10.1016/j.applthermaleng.2009.06.019

Bianco, V., Manca, O., & Nardini, S. (2011). Numerical investigation on nanofluids turbulent convection heat transfer inside a circular tube. *International Journal of Thermal Sciences, 50*, 341–349. doi:10.1016/j.ijthermalsci.2010.03.008

Das, S. K., Choi, S. U. S., & Patel, H. E. (2006). Heat transfer in nanofluids-A review. *Journal of Heat Transfer Engineering, 27*, 3-19. doi:10.1080/01457630600904593

Das, S. K., Putra, N., Thiesen, P., & Roetzel, W. (2003). Temperature dependence of thermal conductivity enhancement for nanofluids. *Journal of Heat Transfer, 125*, 567-574. doi:10.1115/1.1571080

Gnielinski, V. (1976). New equations for heat and mass transfer in turbulent pipe and channel flow. *International Journal of Chemical Engineering, 16*(2), 359-368. doi:10.1252/kakoronbunshu.34.505

Hasan, M. I. (2011). Numerical investigation of counter flow microchannel heat exchanger with MEPCM suspension. *Applied Thermal Engineering, 31*, 1068-1075. doi:10.1016/j.applthermaleng.2010.11.0 32

Heris, S. Z., Etemadand, G., & Esfahany, M. N. (2006). Experimental investigation of oxide nanofluids laminar flow convection heat transfer. *International Communications in Heat and Mass Transfer, 33*, 529–535. doi:10.1016/j.icheatmasstransfer.2006.01.005

Hung, T. C., Yan, W. M., Wang, X. D., & Chang, C. Y. (2012a). Heat transfer enhancement in microchannel heat sinks using nanofluids. *International Journal of Heat and Mass Transfer, 55*, 2559–2570. doi:10.1016/j.ijheatmasstransfer.2012.01.004

Hung, Y. H., Ping, T., & Teng, T. C. (2012b). Assessment of heat dissipation performance for nanofluid. *Applied Thermal Engineering, 32*, 132-140. doi:10.1016/j.applthermaleng.2011.09.008

Lee, J., & Mudawar, I. (2007). Assessment of the effective-ness of nanofluids for single-phase and two-phase heat transfer in micro-channels. *International Journal of Heat and Mass Transfer, 50*, 452-463. doi:10.1016/j.ijheatmasstransfer.2006.08.001

Lee, S., Choi, S. U. S., Li, S., & Eastman, J. A. (1999). Measuring thermal conductivity of fluids containing oxide nanoparticles. *ASME Journal of Heat Transfer, 121*, 280-289. doi:10.1115/1.2825978

Minea, A. A. (2017). Challenges in hybrid nanofluids beha-vior in turbulent flow: Recent research and numerical comparison. *Renewable and Sustainable Energy Reviews, 71*, 426-434. doi:10.1016/j.rser.2016.12.072

Minea, A. A. (2017). Hybrid nanofluids based on Al_2O_3, TiO_2 and SiO_2: Numerical evaluation of different approaches. *International Journal of Heat and Mass Transfer, 104*, 852-860. doi:10.1016/j.ijheatmasstransfer.2016.09.012

Minea, A. A., & Manca, O. (2017). Field-synergy and figure-of-merit analysis of two oxide–water-based nanofluids' flow in heated tubes. *Heat Transfer Engineering, 38*(10), 909-918. doi:10.1080/01457632.2016.1212569

Morini, G. L. (2004). Single-phase convective heat transfer in microchannels: A review of experimental results. *International Journal of Thermal Sciences, 43*, 631-651. doi:10.1016/j.ijthermalsci.2004.01.003

Morini, G. L. (2006). Scaling effects for liquid flows in microchannels. *Heat Transfer Engineering, 27*, 64-73. doi:10.1080/01457630500523865

Pak, B. C., & Cho, Y. I. (1998). Hydrodynamic and heat transfer study of dispersed fluids with submicron metallic oxide particles. *Experimental Heat Transfer, an International Journal, 11*, 151-170. doi:10.1080/08916159808946559

Peyghambarzadeh, S. M., & Hashemabadi, S. H. (2011). Experimental study of heat transfer enhancement using water/ethylene glycol based nanofluids as a new coolent for car radiator. *International Communication in Heat and Mass Transfer, 38*, 1283-1290. doi:10.1016/j.icheatmasstransfer.2011.07.001

Raja, M., Arunachalam, R. M., & Suresh, S. (2012). Experimental studies on heat transfer of alumina/water nanofluid in a shell and tube heat exchanger with wire coil insert. *International Journal of Mechanical and Materials Engineering, 7*(1), 16-23.

Wen, D. S., & Ding, Y. L. (2005). Experimental investigation into the pool boiling heat transfer of aqueous based alumina nanofluids. *Journal of Nanoparticle Research, 7*, 265-274. doi:10.1007/s11051-005-3478-9

Xuan, Y. M., & Li, Q. (2003). Investigation on convective heat transfer and flow features of nanofluids. *ASME Journal of Heat Transfer, 125*, 151-155. doi:10.1115/1.1532008

Appendix

Nomenclature

C_p	Specific heat (J/kg K)
D	Diameter (m)
F	external body force (N)
g	acceleration due to gravity (m/s^2)
h	heat transfer coefficient (W/m^2K)
I	unit tensor
$\overrightarrow{J_I}$	diffusion flux
L	length (m)
m	mass (kg)
Nu	Nusselt Number
p	static pressure (Pa)
Pe	Pecelt Number
Pr	Prandtl Number
Re	Reynolds Number
S_h	heat of chemical reaction
T	temperature (K)
t	time (s)
v	velocity (m/s)
x	axial distance (m)
y	radial distance (m)
Greek	
ρ	density (kg/m^3)
κ	thermal conductivity (W/mK)
μ	viscosity (Ns/m^2)
$\bar{\bar{\tau}}$	stress tensor
ε	Rate of dissipation, J/kg.s
ν	Kinematic viscosity, m^2/s
ϕ	Volume concentration
Subscript	
eff	effective
f	fluid
in	Channel inlet
nf	nanofluid
out	Channel outlet
p	constant pressure
r	radial
ref	reference
t	turbulent